Gas-Phase Conformations of 3-Buten-2-ol from Density-Functional Theoretical Results Together with Electron-Diffraction and Vibrational Spectroscopic Data

I. F. Shishkov,† S. Shlykov,‡ B. Rousseau, Z. H. Peng, C. Van Alsenoy, and H. J. Geise*

Department of Chemistry, University of Antwerpen (UIA), Universiteitsplein 1, B-2610 Wilrijk, Belgium

O. N. Kataeva

A.E. Arbuzov Institute of Organic and Physical Chemistry, Russian Academy of Sciences, A.E. Arbuzov street 8, Kazan 420083, Russia

W. A. Herrebout and B. Van der Veken

Department of Chemistry, University of Antwerp (RUCA), Groenenborgerlaan 171, B-2020 Antwerpen, Belgium

Received: July 24, 2000; In Final Form: November 13, 2000

The conformational space of 3-buten-2-ol (BUO), governed by the torsion angles φ_1(O−C−C=C) and φ_2-(H−O−C−C(sp^2)), was searched, and nine energy minima were located, using the B3LYP/6-31**G approach. Then, geometries of these nine and the vibrational characteristics of the four lowest energy forms were calculated. Experimental evidence of the latter four conformers in the gas phase was obtained from IR frequencies, band intensities, and band shapes measured at room temperature. Analysis of electron-diffraction intensities also measured at room temperature gave the following abundancies (with nomenclature pertinent to the *S* configuration): (+*ac*, −*sc*), 58%; (*sp*, −*sc*) and (*sp*, +*sc*) together, 32%; (−*ac*, +*sc*), 10%. The energy sequence as well as conformationally induced variations in bond lengths, valence angles, and OH frequencies could be rationalized by attractive (hyper)conjugative and repulsive steric effects operative in BUO. The intermediacy of BUO between allyl alcohol and 1-butene shows in the observation that C2−H, C2−OH, and C2−CH$_3$ eclipse the C=C bond in the (+*ac*, xx), (*sp*, xx), and (−*ac*, xx) conformers, respectively. In all four conformers, OH points toward C=C, indicative of an attractive intramolecular OH/π (C=C) interaction. Experimental and calculated wavenumbers of the individual conformers could be matched satisfactorily, after scaling the four B3LYP force fields using only three transferable scale factors published by Rauhut and Pulay (*J. Phys. Chem.* **1995**, *99*, 3093).

Introduction

In research programs of small gas-phase alcohols and their derivatives, 3-buten-2-ol (BUO) has been given much attention.[1−5] Being a small molecule, it can serve as a model compound to study stereoelectronic effects, as well as the possibility of intramolecular hydrogen bonding. The two axes of internal rotation and the chiral substitution near the double bond make the molecule interesting for conformational analysis. Taking into account the usual tendency of single and double bonds to eclipse one another, one envisages three potential forms determined by φ_1(O−C−C=C). With the *S* configuration as the starting point, they are +*ac* (anticlinal; C−H eclipses the double bond), −*ac* (C−CH$_3$ eclipses), and *sp* (synperiplanar; C−OH eclipses). For each of these, there are three possible orientations of the hydroxyl group with respect to the C−C(sp^2) bond: +*sc* (synclinal), −*sc*, and *ap* (antiperiplanar), determined by φ_2(H−O−C−C(sp^2)). Figure 1 shows the nine possible BUO conformations with the *S* configuration at C2 and gives the IUPAC nomenclature.[6]

In previous investigations, Kahn et al.[2,3] calculated on the theoretical side the conformational profile of BUO with standard ab initio methods on the 6-31G*//3-21 G level. All nine conformers were analyzed. The three forms with the lowest energy were (+*ac*, −*sc*), (*sp*, −*sc*), and (*sp*, +*sc*), with calculated relative energies of 0, 0.6, and 0.8 kcal/mol, respectively. In this, BUO resembles allyl alcohol,[7−9] in which similar forms occur. The next three BUO conformers were calculated to be 1.6 (*sp*, *ap*), 1.9 (+*ac*, +*sc*), and 2.7 kcal/mol (+*ac*, *ap*) above the (+*ac*, −*sc*) conformation. The three forms in which the bond to the terminal methyl group eclipses the double bond were no minima on the energy surface. In this, BUO seemed to differ from 1-butene, which in the gas phase contains as much as 17% of the form, with C−CH$_3$ eclipsing the double bond.[10,11]

On the experimental side, the microwave spectra of BUO, CH$_2$=CHCH(OH)CH$_3$, and CH$_2$=CHCH(OD)CH$_3$ have been investigated by Smith et al.[1] More than two conformers were believed to be present, but only two could be assigned. In terms of the *S* configuration, the predominant conformer was shown to be (+*ac*, −*sc*), with the hydrogen atom at C2 eclipsing the double bond, the methyl carbon being about −118° from the syn position, and the oxygen atom being about +122° from the syn position. The other assigned conformer was (*sp*, +*sc*). It has the C−O eclipsing the double bond ($\varphi_1 = 4°$) and the methyl

* To whom correspondence should be addressed.
† On leave from Department of Chemistry, Moscow State University (MSU), Leninskiye Gori, Moscow 119899, Russia.
‡ On leave from the Academy of Chemical Technology, Department of Physics, Engels street 7, Ivanovo 153460, Russia.

10.1021/jp002616g CCC: $20.00
Published on Web 01/19/2001

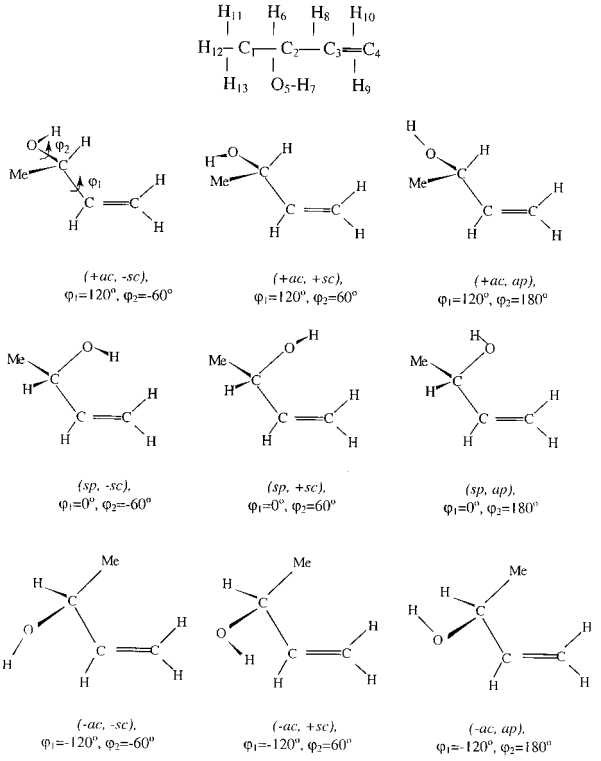

Figure 1. Possible conformers of (*S*)-3-buten-2-ol, together with atomic numbering and IUPAC nomenclature.[6]

carbon +124° away form the syn position. Relative intensity measurements gave the energy difference between the lowest rotational levels of these two conformers as 0.52(14) kcal/mol. The authors find additional evidence for the second conformer in the vapor-phase IR spectrum: they consider the observed difference of 12 cm^{-1} between two OH stretching frequencies too small to be a P−R splitting, although no calculations of P−R splitting were performed. Still, a good many moderately strong microwave lines remained unidentified, suggesting the presence of further unknown rotamer(s).

So, despite the seeming simplicity of BUO and the large attention it has received, the conformational composition of this molecule in the gas phase has not yet been determined unambiguously. Therefore, the aim of this work is threefold: (i) the determination of the number, energy sequence, and geometry of the BUO conformers in the gas-phase on the basis of theoretical calculations, spectroscopic measurements, and electron-diffraction intensities, (ii) the determination of reliable force fields from calculations using the B3LYP/6-31G** basis set, and (iii) the creation of a self-consistent molecular model which is simultaneously in agreement with the new electron-diffraction experiment and the new gas-phase IR spectra. The self-consistent molecular approach provides a view on a molecule that agrees with all gas-phase data available at the present time and has proved useful in a growing number of cases.[11−24]

Experimental Section

A commercial sample (Janssen Chimica) with a reported purity of 99% was used without further purification to obtain electron-diffraction intensities and new high-resolution IR spectra.

Gas Electron Diffraction. Diffraction patterns were recorded photographically on the Antwerpen diffraction unit (manufactured by Technisch Physische Dienst, TPD-TNO, Delft, The Netherlands).[25] For the gas electron-diffraction experiments, the temperature of the nozzle was kept at 300 K. An accelerating voltage of 59.88 kV was used, stabilized within 0.01% during exposures. The corresponding electron wavelength was calibrated against the known[26] CC bond length of benzene and resulted in $\lambda = 0.048\ 71(3)$ Å. Recordings were taken at three nozzle-to-photographic plate distances: 59.982(2) (four plates), 35.104(2) (five plates), and 19.980(2) cm (four plates). Optical densities were measured on a modified[27] rotating ELSCAN E-2500 densitometer. Density values were converted to intensities using the one-hit model of Forster.[28] Coherent scattering factors were taken from Ross et al.[29] and incoherent scattering factors from Tavard et al.[30] The data were processed by standard procedures.[31]

The experiment yielded leveled intensities in the following ranges: 60 cm, $3.50 \le s \le 11.50$ $Å^{-1}$; 35 cm, $7.00 \le s \le 19.50$ $Å^{-1}$; 20 cm, $12.00 \le s \le 33.50$ $Å^{-1}$ (all with $\Delta s = 0.25$ $Å^{-1}$). Leveled intensities $I(s)$ with final backgrounds $B(s)$ and the resulting $sM(s)$ curve are shown in Figures 2 and 3.

Infrared Spectroscopy. The vapor-phase infrared spectrum of BUO was recorded at room temperature on a Bruker IFS 113v spectrometer equipped with a globar source, a Ge/KBr beam splitter, and a broad-band mercury cadmium telluride detector. The compound was contained in a 29 cm gas cell with KBr windows at a pressure of 15 mbar. A total of 200 scans for both the reference and sample were accumulated, Happ−Genzel apodized, and Fourier transformed using a zero-filling factor of 4 to produce a spectrum with a resolution of 0.5 cm^{-1}. Prior to recording the spectrum, the compound was dried over molecular sieves. Despite this, very weak bands due to water vapor could still be detected in the spectrum.

Theoretical Calculations

Ab initio calculations were carried out using Pulay's gradient method[32−34] and the program BRABO.[35] Density-functional theory (DFT) calculations were performed with the Gaussian 94 program.[36] Knowing that for allylic alcohols[11,37] the energy content and even the sequence of conformers strongly depend on the level of sophistication, we used in ab initio the 4-21G[38] and the 6-31G** basis sets.[39,40] For the DFT calculations, we chose the B3LYP hybrid functional, made up of the Becke exchange functional,[41] the correlation functional of Lee et al.,[42] and the Hartree−Fock exchange term.[43−45] The basis set chosen was 6-31G**. Convergence criteria were chosen in conformity with ref 46 for the 4-21G and 6-31G** calculations, whereas the standard criteria implemented in the Gaussian 94 program[36] were used for the DFT calculations. Figure 4 shows the φ_1 and φ_2 energy plot at the B3LYP/6-31G** level calculated in steps of 30° in φ_1 and φ_2 and with full relaxation of all other geometrical parameters. Table 1 gives the relative energies for all conformers calculated at the three levels, together with the gas-phase conformer composition at 300 K predicted by the DFT calculations. It should be noted (Table 1) that the 6-31G** and B3LYP/6-31G** relative energy sequences at this point are still in agreement with the limited experimental data sofar available, but the 4-21G sequence is not. The ab initio and DFT calculations differ, however, strongly in treating the high-energy forms (−*ac*, −*sc*), (−*ac*, +*sc*), and (−*ac*, *ap*). At the B3LYP/6-31G** level, the latter forms are energy minima and the (−*ac*, +*sc*) form is predicted as the fourth stable conformer present in the gas phase at 300 K in about 6%. This result brings the conformational behavior of BUO and 1-butene in line with one another. Also, at the DFT level, the calculated dipole moments of the two lowest energy conformers ((*ac*, −*sc*), 1.39

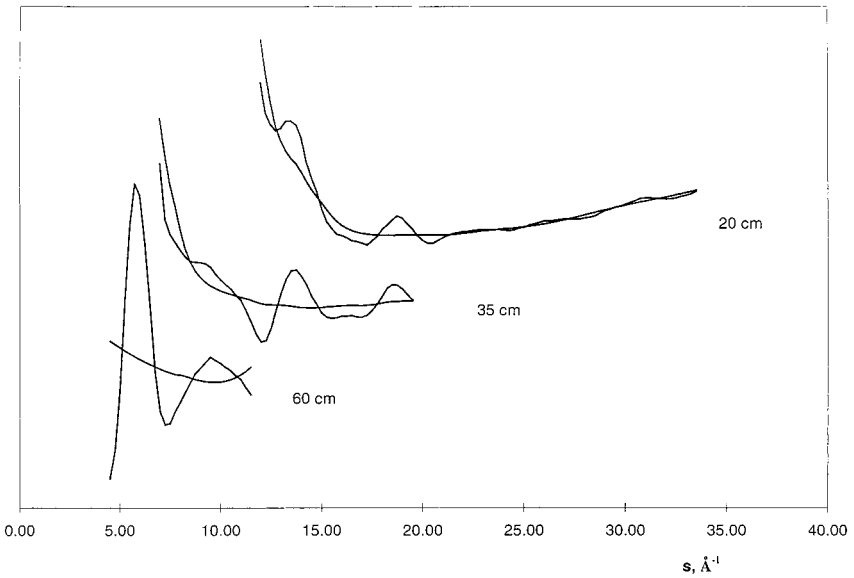

Figure 2. Experimental leveled intensities, $I(s)$, with final backgrounds, $B(s)$, obtained for BUO in the electron-diffraction experiments.

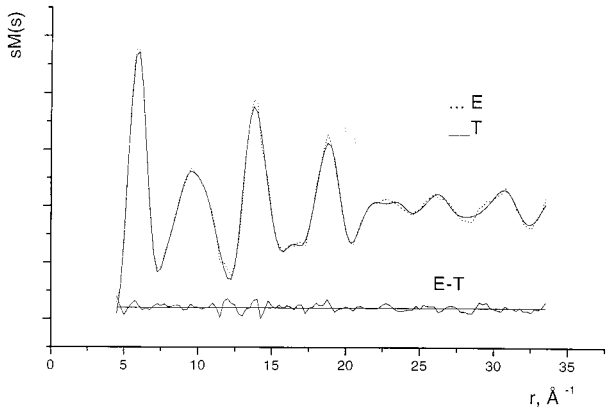

Figure 3. Experimental (· · ·) and theoretical (—) $sM(s)$ curve obtained for BUO in the electron-diffraction experiments, together with the final difference curve experimental minus theoretical $sM(s)$.

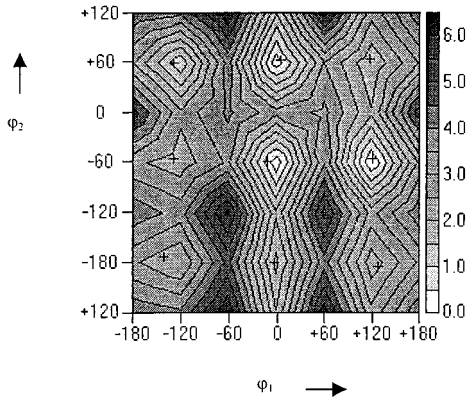

Figure 4. Conformational energy map of BUO as a function of φ_1 and φ_2, resulting from B3LYP/6-31G** calculations in steps of 30° in φ_1 and φ_2. Crosses (+) indicate the positions of the nine possible conformers. The gray scale (on the right) denotes kcal/mol, and the separation between contour lines is 0.5 kcal/mol.

D; (*sp*, −*sc*), 1.40 D) are close to the only available experimental value (1.41 D[1]).

The equilibrium geometries (r_e-type) of the nine BUO forms, calculated at the B3LYP/6-31G** level, are given in Table 2. In passing, we note here that the application of the multiplicative corrections of De Smedt et al.[21] to the r_e(4-21G) bond distances

TABLE 1: Ab Initio Calculated Relative Energies (kcal/mol) of BUO Conformers and DFT-Based Conformer Composition (%) at Room Temperature

conformer	4-21G	6-31G**	B3LYP/6-31G**	comp., %
(+*ac*, −*sc*)	0	0	0	33.5
(*sp*, −*sc*)	−0.43	0.07	0.13	27.0
(*sp*, +*sc*)	−0.34	0.37	0.18	24.8
(−*ac*, +*sc*)			1.07	5.6
(*sp*, *ap*)	0.78	1.18	1.34	3.6
(+*ac*, +*sc*)	1.76	1.81	1.57	2.4
(+*ac*, *ap*)	1.53	1.55	1.68	2.0
(−*ac*, *ap*)			2.45	0.6
(−*ac*, −*sc*)			2.70	0.4

resulted in r_g(4-21G) bond lengths very close to the r_e(B3LYP) lengths. The root-mean-square deviation over the four most abundant rotamers is only 0.003 Å. These empirical corrections were formulated at the time and have since proved very efficient to counteract the systematic errors in 4-21G bond lengths, because of basis set truncation, and particularly the neglect of electron correlation. Hence, the observation strongly suggests that an r_e(B3LYP/6-31G**) length directly represents an r_g bond length.

Thus, we confine ourselves to a discussion of B3LYP conformations and geometries. The behavior of φ_1, governing the main skeleton, can be visualized in terms of (hyper)-conjugative effects somewhat modified by steric hindrance. The (hyper)conjugative effect is maximally effective when the C−X (X = H6, CH_3 (Me), OH) bond is coplanar (eclipses) with the C═C bond. It should decrease the C−X bond length and increase the X−C2−C3 valence angle. Moreover, the decrease and increase in function of X should follow the (hyper)-conjugative strength of X as expressed in Hammett's σ values, i.e., in the order of H < CH_3 < OH. To check on this, we take the decrease of the C−X length as the CX length averaged over the corresponding eclipsed conformations minus the CX length averaged over the remaining not eclipsed forms. The increase of the X−C2−C3 angle is similarly defined. Three conformers, in which the "trans rule" (see below) interferes with the eclipse effects, were omitted from the averages. The results, given in Table 3A, are in excellent agreement with expectations. The data show the competing influence of CH_3 steric hindrance to grow from small in bond lengths, to medium in valence angles, to important in torsion angles and conformational equilibria.

TABLE 2: Optimized Geometries (r_e-Type) of the Nine BUO Conformations Calculated at the B3LYP/6-31G Level**

	(+*ac*, −*sc*)	(*sp*, −*sc*)	(*sp*, +*sc*)	(−*ac*, +*sc*)	(*sp*, *ap*)	(+*ac*, +*sc*)	(+*ac*, *ap*)	(−*ac*, *ap*)	(−*ac*, −*sc*)
relative energy (kcal/mol)	0	0.13	0.18	1.07	1.34	1.57	1.68	2.45	2.70
total dipole moment (D)	1.38	1.40	1.54	1.48	1.73	1.62	1.64	1.63	1.46
Bond Lengths (Å)									
C2−C1	1.526	1.530	1.535	1.528	1.536	1.532	1.534	1.528	1.522
C3−C2	1.507	1.512	1.513	1.511	1.506	1.509	1.505	1.508	1.513
C4−C3	1.333	1.332	1.332	1.333	1.331	1.332	1.331	1.332	1.332
O5−C2	1.434	1.424	1.424	1.436	1.424	1.434	1.431	1.434	1.435
H6−C2	1.103	1.105	1.099	1.098	1.106	1.096	1.102	1.106	1.105
H7−O5	0.967	0.967	0.968	0.968	0.965	0.967	0.967	0.966	0.966
H8−C3	1.090	1.090	1.090	1.090	1.090	1.093	1.090	1.089	1.093
H9−C4	1.088	1.086	1.086	1.086	1.084	1.087	1.088	1.086	1.086
H10−C4	1.086	1.085	1.085	1.086	1.086	1.086	1.086	1.086	1.086
H11−C1	1.094	1.093	1.093	1.093	1.097	1.094	1.097	1.096	1.093
H12−C1	1.094	1.094	1.095	1.095	1.095	1.095	1.094	1.094	1.093
H13−C1	1.094	1.094	1.097	1.096	1.094	1.098	1.095	1.093	1.094
Valence Angles (deg)									
C3−C2−C1	112.5	111.7	111.6	115.3	111.3	112.0	111.5	115.0	115.0
C4−C3−C2	124.7	124.8	124.6	127.0	125.2	125.1	124.7	126.9	127.3
O5−C2−C1	106.1	106.6	111.3	111.2	111.2	110.8	110.8	111.2	106.3
O5−C2−C3	110.3	112.9	112.7	109.4	108.8	111.2	106.6	105.7	110.4
H6−C2−C1	109.0	107.9	108.1	108.5	108.0	109.2	108.9	108.5	108.3
H6−C2−C3	108.7	107.7	108.3	108.0	107.6	108.8	108.7	107.2	107.5
H6−C2−O5	110.2	109.9	104.4	103.6	109.9	104.5	110.4	109.1	109.1
H7−O5−C2	107.2	107.3	106.9	106.7	107.6	107.4	107.5	107.4	108.0
H8−C3−C2	115.0	115.2	115.4	113.5	114.5	115.3	114.7	113.3	114.2
H8−C3−C4	120.3	120.0	120.0	119.5	120.3	119.6	120.5	119.8	118.6
H9−C4−C3	121.5	121.1	121.0	122.4	121.1	121.5	121.6	122.6	122.3
H10−C4−C3	122.0	121.7	121.7	121.3	121.3	122.0	121.8	121.1	121.3
H10−C4−H9	116.5	117.2	117.3	116.3	117.7	116.6	116.6	116.3	116.4
H11−C1−C2	109.9	110.1	110.1	109.4	110.8	110.0	110.7	110.2	109.4
H12−C1−C2	110.7	110.9	111.3	111.6	111.3	111.3	111.1	111.6	111.1
H12−C1−H11	109.0	108.7	108.6	108.5	107.6	108.9	107.9	107.4	108.5
H13−C1−C2	110.3	109.7	110.6	111.1	109.9	110.7	110.3	110.3	110.4
H13−C1−H11	108.2	108.8	108.5	108.2	108.6	108.2	108.1	108.4	108.3
H13−C1−H12	108.7	108.6	107.7	108.0	108.6	107.6	108.6	108.9	109.0
Torsion Angles (deg)									
C3−C2−C1−H11	−177.1	177.8	178.8	−178.0	177.4	−178.0	−178.5	−178.7	−177.8
O5−C2−C1−H11	−56.3	−58.4	−54.3	−52.7	−61.1	−53.3	−59.9	−58.6	−55.3
H6−C2−C1−H11	62.3	59.6	59.8	60.7	59.6	61.3	61.6	61.3	61.9
C3−C2−C1−H12	62.5	57.5	58.4	61.9	57.8	61.2	61.7	62.1	62.4
O5−C2−C1−H12	−176.8	178.7	−174.8	−172.7	179.3	−174.1	−179.8	177.8	−175.1
H6−C2−C1−H12	−58.1	−60.7	−60.7	−59.4	−60.0	−59.5	−58.2	−57.9	−58.0
C3−C2−C1−H13	−57.9	−62.5	−61.3	−58.6	−62.5	−58.5	−58.8	−59.0	−58.7
O5−C2−C1−H13	62.8	61.3	65.6	66.7	58.9	66.3	59.7	61.0	63.8
H6−C2−C1−H13	−178.5	179.3	179.7	−180.0	179.6	−179.1	−178.8	−179.0	−179.0
C4−C3−C2−C1	−121.0	110.0	132.6	−2.9	121.8	−118.0	−110.2	−14.9	−7.2
C4−C3−C2−O5	120.7	−10.2	6.5	−129.1	−1.1	117.5	128.8	−138.0	−127.5
C4−C3−C2−H6	−0.2	−131.7	−108.5	118.7	−120.1	2.9	9.8	105.8	113.5
H8−C3−C2−C1	60.0	−69.8	−47.1	175.7	−58.0	61.7	68.5	166.0	173.4
H8−C3−C2−O5	−58.3	170.1	−173.2	49.5	179.2	−62.9	−52.5	42.9	53.2
H8−C3−C2−H6	−179.2	48.5	71.8	−62.7	60.2	−117.5	−171.4	−73.3	−65.8
H9−C4−C3−C2	0.9	−0.8	1.8	−1.5	0.6	−0.3	−2.0	1.2	0.2
H9−C4−C3−H8	179.8	179.0	−178.5	180.0	−179.7	−180.0	179.3	−179.7	179.5
H10−C4−C3−C2	−179.6	−179.8	−179.4	179.0	−179.6	179.7	178.0	−178.6	−179.6
H10−C4−C3−H8	−0.7	−0.1	0.3	0.5	0.1	0.0	−0.7	0.5	−0.4
H7−O5−C2−C1	176.7	179.4	−63.9	−69.1	57.7	−61.3	53.6	62.0	179.7
H7−O5−C2−C3	−54.6	−57.5	62.4	59.5	−179.3	63.9	175.1	−172.5	−54.9
H7−O5−C2−H6	65.5	62.7	179.7	174.5	−61.8	−178.9	−67.1	−57.6	63.1

The C−X bond length decrease is considerably smaller for X = CH_3 than for X = OH, but the X−C−C angle increase for X = CH_3 is almost equal to that of X = OH, and the destabilizing CH_3 hindrance changed the order of conformer abundancy into C−CH_3 eclipsed < C−H eclipsed < C−OH eclipsed. The torsion angle φ_2(H−O−C2−C3) is held responsible for the fine-tuning of the BUO conformers. The simplest way to visualize the results here is in terms of repulsive bond−bond interactions of OH/CH and OH/C−Me, modified by an attractive interaction between OH and C═C of type σ^*(OH)/π(C═C), as is depicted in Figure 5. The latter interaction, although weak, is decisive in tipping the energy balance in favor of the (+*ac*, −*sc*), (*sp*, −*sc*), (*sp*, +*sc*), and (−*ac*, +*sc*) conformers, and this, together with the repulsion OH/C−Me being larger than that of OH/C−H, predicts the energy order qualitatively. The repulsive interactions show in a series of geometrical details the following generalized trans rule[47] for alcohols: if in a conformation a CH or CC bond is *ap* to the OH bond, then the CH or CC bond length is smaller and also the OCH or OCC angle is smaller than in those cases where the bond is *sc* to the OH bond. This is observed to hold (Table 2) for (i) the C2−C3 bond length and O−C2−C3 angle in all (xx, *ap*) conformers, (ii) the C2−H6 bond length and the O−C2−H6 angle in all (xx, +*sc*) conformers, and (iii) the C1−

TABLE 3: Geometrical Consequences[a] of (Hyper)conjugative Effects (A) and of σ^*(OH)/π(C=C) Interaction (B and C) on BUO Conformations (see the text)

A

X		avg; eclipsed	avg; not eclipsed	effect
H	C2−H6	1.1025	1.1033	−0.0008
CH_3	C2−C1	1.5276	1.5321	−0.0045
OH	C2−O5	1.4235	1.4339	−0.0104
H	H−C2−C3	108.75	107.72	+1.03
CH_3	C1−C2−C3	115.12	111.78	+3.34
OH	O5−C2−C3	112.81	108.92	+3.89

B

	H-bridged	not H-bridged
O5−H7	0.9673	0.9664
C3=C4	1.3326	1.3315
H7−O5−C2	107.03	107.59
H7−O5−C2−C3	58.49	59.39

C

	(+*ac*, −*sc*)	(*sp*, −*sc*)	(−*ac*, +*sc*)	(*sp*, +*sc*)
O5−H7	0.9666	0.9669	0.9677	0.9680
$\|\varphi_2$(H−O−C−C)$\|$	54.6	57.5	59.5	62.4
υ(OH)	3648	3644	3630	3626

[a] Distances in angstroms, valence and torsion angles in degrees, and frequencies in reciprocal centimeters.

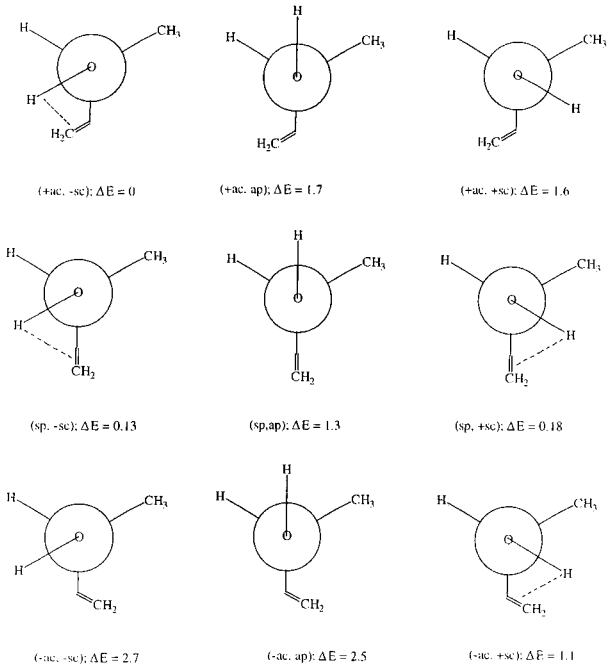

Figure 5. Newman projections along the bond O−C(2) showing repulsive bond−bond (H/H and H/CH_3) and attractive (OH/C=C) interactions (dashed lines), together with relative energies of conformers.

C2 bond length and O−C2−C1 angle in all (xx, −*sc*) conformers. Interestingly, when the trans rule is in conflict with the eclipse rule, as it is for the O−C2−C3 angle in (*sp*, +*ac*), the value (108.8°) is intermediate in the total angle range (105.6−112.9). When the rules reinforce each other, as they do for the C2−H6 length in (+*ac*, +*sc*) and for the C1−C2 length in (−*ac*, −*sc*), the values are the next-to-smallest and the smallest, respectively. Finally, the attractive OH/π(C3=C4) interaction contains[48] a dispersion and a delocalization component. The latter, being of the σ^*(OH)/π(C=C) type, elongates the OH bond length somewhat. This shows when we compare the OH length averaged over the four lowest energy ("H-bridged") conformers

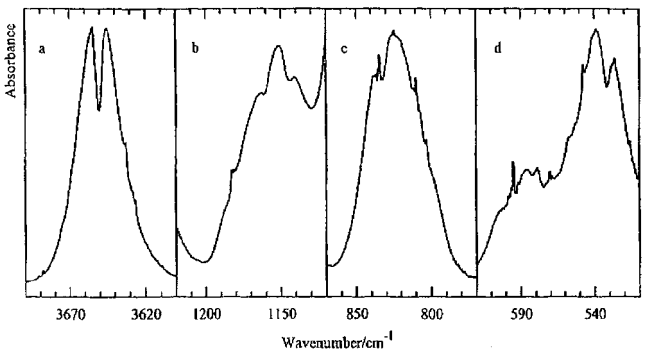

Figure 6. Details of the room-temperature vapor-phase IR spectrum of BUO. See the text for explanations. The absorbance scales have been adjusted for the individual details. Therefore, band heights in the individual details do not reflect relative intensities.

(0.9673 Å) with the OH length averaged over the five other ("not H-bridged") conformers (0.9664 Å). Similarly, in the "bridged" forms, the averaged C=C length is larger and the averaged H−O−C(2) valence angle as well as the averaged H−O−C(2)−C(3) torsion angle is smaller than those in the not-bridged forms (Table 3B).

Furthermore, Figure 5 reveals that the overlap σ^*(OH)/π-(C=C) requires a *sc* orientation of OH with respect to C2−C3. The CH_3 group polarizes the π(C=C) cloud such that a better overlap occurs with a σ^*(OH) in the −*sc* orientation than in the +*sc* orientation. Also, it may be seen that in the (*ac*, xx) forms the OH direction is better suited for overlap than that in the (*sp*, xx) forms. It follows that the OH/π(C=C) interaction decreases in the order of (*ac*, −*sc*) > (*sp*, −*sc*) > (−*ac*, +*sc*) > (*sp*, +*sc*). Then, the OH bond weakens in that order, the OH bond length increases, and the υ(OH) stretching frequency decreases. These features are indeed reflected in the calculated data (Table 3,C). Moreover, we see (Table 3C) an increase of the torsion angle $|\varphi_2$(H−O−C−C(sp^2))$|$ in the same order. This may indicate the existence of a competition for the OH interaction between the π(C=C) and π(CH_3) system, the latter being possible in the (xx, +*sc*) forms and not in the (xx, −*sc*) forms.

Vibrational Spectroscopy

The Cartesian harmonic force fields of the four most abundant conformations were calculated at the DFT-B3LYP/6-31G** level using the analytical method and default parameters available in the Gaussian 94 program. Rauhut and Pulay[49] have shown recently that such force fields, particularly after some additional scaling, form a reliable basis for the interpretation of complex experimental IR spectra. They also provided a small number of transferable scaling factors applicable to a variety of organic compounds. We took three of their values to scale the stretching, bending, and torsion force constants, respectively, of the four BUO conformers. Next, we calculated vibrational frequencies as well as band intensities, band types, and potential energy distributions, which led to the assignment of the complex experimental gas-phase IR spectrum discussed below. The calculated data and the frequencies observed for the dominant conformer have been collected in Table 4.

The region of the O−H stretching is shown in Figure 6a. The spectrum is dominated by two maxima at 3656 and 3645 cm^{-1}. The presence of the two maxima was interpreted by Smith et al. as evidence for the presence of a conformational equilibrium, because the difference of 12 cm^{-1} between the maxima was considered too small to be a PR separation.[1] However, the contour suggests that the two maxima are the PQ

TABLE 4: Experimental (exp) Wavenumbers (cm^{-1}), Calculated (calc) Wavenumbers, and Calculated Band Intensities (int, 10^6 cm/mol) of the Four Lowest Energy BUO Conformers, as Well as IR Assignments for the (+*ac*, −*sc*) Conformer

	(+ac, −sc)				(sp, −sc)		(sp, +sc)		(−ac, +sc)	
no.	exp	calc	int	assignment	calc	int	calc	int	calc	int
1	3650	3647	1.09	υ(OH)	3644	1.02	3626	0.86	3630	0.99
2	3090	3097	1.74	υ_{as}(=CH_2)	3111	1.15	3112	1.10	3104	1.65
3	3022	3019	0.40	υ_{sym}(=CH_2)	3031	0.48	3031	0.57	3030	0.53
4	2991	3010	2.43	υ(=CH)	3013	2.52	3014	2.06	3018	1.65
5	2991	3004	2.08	υ_{as}(CH_3)	3007	2.25	3002	2.42	3005	2.03
6	2984	2997	2.27	υ_{as}(CH_3)	3000	1.80	2979	3.92	2985	4.19
7	2939	2924	1.58	υ_{sym}(CH_3)	2926	1.84	2911	1.79	2916	1.25
8	2878	2903	4.66	υ(CH)	2873	6.33	2950	1.42	2956	1.51
9	1654	1659	0.16	υ(C=C)	1658	0.49	1658	0.36	1659	0.39
10	0	1475	0.09	δ_{as}(CH_3)	1476	0.20	1473	0.14	1475	0.28
11	1455	1462	0.55	δ_{as}(CH_3)	1462	0.27	1469	0.53	1472	0.63
12	1428	1430	1.48	scissoring =CH_2	1411	0.45	1410	0.55	1423	0.99
13	1386	1391	1.42	δ_{sym}(CH_3)	1389	0.80	1379	0.55	1380	2.62
14	1374	1360	1.16	C2 angle bending	1365	0.10	1385	4.36	1384	3.61
15	1318	1322	1.83	C2 angle bending	1341	3.64	1306	0.63	1339	1.41
16	1284	1280	0.16	δ(=CH)	1281	0.40	1284	0.80	1289	0.00
17	1251	1249	6.61	δ(C−O−H)	1252	5.15	1262	0.63	1246	0.79
18	1183	1169	0.76	skeletal vibration	1146	1.54	1129	5.69	1136	0.42
19	1105	1096	2.45	skeletal vibration	1062	1.73	1062	1.47	1089	4.91
20	1023	1025	0.21	τ(C=C) and C3H oop	1029	0.98	1029	2.42	1032	2.25
21	1046	1017	7.10	skeletal vibration	1013	1.89	1019	1.70	1011	5.39
22	995	969	1.05	ρ_t(=CH_2)	986	3.94	987	2.64	986	1.45
23	923	942	3.41	wag =CH_2 and =CH oop	938	2.93	940	3.01	941	3.28
24	920	909	2.44	skeletal vibration	911	1.10	905	0.62	897	1.15
25	834	813	0.18	skeletal vibration	784	0.14	780	0.75	790	1.30
26	686	690	0.83	τ(C=C) and =C3H oop	677	1.45	670	0.82	678	0.57
27	532	522	0.94	skeletal vibration	591	0.46	566	1.52	518	0.39
28	0	372	3.04	skeletal vibration	424	1.29	426	0.65	409	2.79
29	0	352	8.54	τ(HO−C2−C3)	364	9.58	371	5.77	382	3.02
30	0	322	1.19	skeletal vibration	325	2.78	321	5.28	336	6.86
31	0	310	0.04	skeletal vibration	279	0.04	277	0.24	277	0.09
32	0	233	0.07	τ(C−CH_3)	242	0.11	251	0.03	266	0.08
33	0	104	0.08	τ(O−C2−C3=C)	127	0.09	122	0.14	107	0.15

and QR branches of a type-B band. To confirm this, we have performed rigid asymmetric top contour simulations[50] for the more likely four lower energy conformers, using the rotational constants from the DFT calculations. We found that for each of the conformers the pure type-B transition shows a contour very similar to the experimental υ(OH) contour. Therefore, the presence of the two maxima cannot be taken to show the presence of a conformational equilibrium but rather must be due to the occurrence of a single type-B transition, with band center at 3650 cm^{-1}. Because of the similarity of the calculated type-B contours for the different conformers, the conformer giving rise to the experimental type-B contour cannot be identified using characteristics such as the PQ−QR separation. Fortunately, the O−H stretching is a well-localized vibration, and for these the vapor-phase contour can be predicted using the bond dipole (BD) model,[50] in which it is assumed that the dipole gradient $(\delta\bar{\mu}/\delta Q)_0$ is parallel to the bond which is being stretched. For O−H stretches, it has been shown that the gradient may not be completely parallel to the O−H bond but may be at an angle of up to 20°.[51] Within the BD model, the O−H stretching should be predominantly type-B for (+*ac*, −*sc*), for (*sp*, −*sc*), it should be a hybrid with similar contributions of types A−C, and for (*sp*, +*sc*) and (−*ac*, +*sc*), it should be a virtually pure type-C transition. Only when the dipole gradient would be about perpendicular to the OH bond would a type-B bond occur for (*sp*, +*ac*) and (−*ac*, +*ac*). Because it is extremely unlikely that this is the case, the latter two conformers cannot reproduce the observed type-B band, and these conformers must be rejected as candidates for the 3650 cm^{-1} transition. The hybrid calculated for (*sp*, −*sc*) contains a pronounced Q branch, which cannot be removed by rotating the dipole gradient away from the O−H bond orientation by 15−20°. Therefore, it is also unlikely that the 3650 cm^{-1} band is due to the (*sp*, −*ac*) conformer. This leaves the (+*ac*, −*sc*) conformer: the BD hybrid contains a weak Q branch, which disappears when the dipole gradient is rotated by some 10° away from the O−H bond, in the direction of the *b* axis. Hence, within the boundaries set by the experiment,[51] this conformer reproduces the experimental υ(OH) contour. Therefore, the dominant species present in the vapor phase of BUO is identified to have the (+*ac*, −*sc*) conformation.

Apart from the strong type-B transition, several weaker bands can be identified in the same region: a very weak Q branch is present at 3655 cm^{-1}, close to the RQ maximum of the type-B transition, and very weak Q branches are also observed at 3633 and near 3627 cm^{-1}, the latter showing some thermal structure. Although it cannot be ruled out that, in view of their weakness, some of them are combination bands of the dominant conformer, we are inclined to attribute these bands to the presence of several conformers. We assign these weak transitions in the calculated order to the (*sp*, −*sc*), (*sp*, +*sc*), and (−*ac*, +*sc*) conformers. The fact that for each of the observed bands the Q branch dominates the transition is in agreement with the calculated contours discussed above. Because the intensities predicted in Table 4 for υ(OH) do not vary much among the conformers, the weakness of the transitions suggests that the population of the higher energy conformers is significantly smaller than that of the dominant conformer.

The region between 3200 and 2800 cm^{-1} contains the various C−H stretching modes. When four conformers are simultaneously present in the vapor phase, as suggested by the OH stretches, this should contain 28 fundamentals, and the spectrum should be extremely crowded. However, in view of the relative intensities of the OH stretches, it may be expected that also the

CH stretching region is dominated by the bands because of the (+*ac*, −*sc*) conformer, and we will discuss the assignments in light of this conformer first. $\upsilon_{as}(=CH_2)$ is predicted with intermediate intensity at 3097 cm^{-1} and must be associated with the dominant type-C transition at 3090 cm^{-1}. Its symmetric counterpart $\upsilon_{sym}(=CH_2)$ is predicted, with significantly smaller intensity at 3015 cm^{-1}. In this region, two weak Q branches can be distinguished at 3022 and 3015 cm^{-1}. Because $\upsilon_{as}(=CH_2)$ is predominantly type-C, $\upsilon_{sym}(=CH_2)$ should show an A/B hybrid contour. Therefore, we assign this mode to the 3022 cm^{-1} band, because it has a fairly well-defined R branch near 3030 cm^{-1}, whereas for the 3015 cm^{-1} transition, neither P nor R branches can be distinguished, a characteristic of important type-C character.

Three fundamentals, $\upsilon(=CH)$ and both $\upsilon_{as}(CH_3)$'s, are predicted, with considerable intensity in the 3010−2995 cm^{-1} region. Here, only two intense Q branches are observed at 2991 and 2984 cm^{-1}. Because they both have mainly type-C character, we assign them in the calculated order as $\upsilon(=CH)$ and one of the $\upsilon_{as}(CH_3)$, respectively, at the same time assuming that the other $\upsilon_{as}(CH_3)$ is hidden by these two. The assignment of $\upsilon_{sym}(CH_3)$ and $\upsilon(CH)$, predicted at 2924 and 2903 cm^{-1}, is problematic. Near 2936 cm^{-1}, the experimental spectrum shows a broad, relatively weak band with undefined contour, which we tentatively assign to $\upsilon_{sym}(CH_3)$. $\upsilon(CH)$ is predicted to be the most intense transition in this region, but this is not substantiated by the experiment: near 2880 cm^{-1} a broad feature with medium intensity is observed, in which several transitions can be distinguished. Again, tentatively, the maximum with the highest absorbance, at 2878 cm^{-1} is assigned to $\upsilon(CH)$. Apart from the bands assigned above, a number of weak transitions are also observed. For instance, near the 3090 cm^{-1} band assigned to $\upsilon_{as}(=CH_2)$, weak Q branches are present at 3100, 3097, and 3079 cm^{-1}. We interpret them as being due to higher energy conformers, although, in view of their weakness, it again cannot be excluded that some of them are combination bands of the dominant conformer. Because of the complexity of the spectrum in this region and because the number of observed bands due to higher conformers is smaller than that expected, no attempts were made to assign the weak bands in detail.

The contour of $\upsilon(C=C)$, near 1650 cm^{-1}, shows two Q branches at 1654 and 1647 cm^{-1}. With the relative band areas under consideration, the high frequency component is slightly more intense than the other. The calculations predict that this mode in (+*ac*, −*sc*) and (−*ac*, +*sc*) appears accidentally degenerate, at a mere 1 cm^{-1} above the also accidentally degenerate $\upsilon(C=C)$ in (*sp*, −*sc*) and (*sp*, +*sc*). Despite their significantly higher separation, we assign the 1654 cm^{-1} component to the (+*ac*, −*sc*) and (−*ac*, +*sc*) pair and the 1647 cm^{-1} component to the (*sp*, −*sc*) and (*sp*, +*sc*) pair, i.e., in the calculated order. With the help of the conformer composition from the electron-diffraction data (see below), the somewhat higher IR intensity of the 1654 cm^{-1} component is explained by the summed contributions of 60% (+*ac*, −*sc*) with a calculated IR intensity $I(\text{calc}) = 0.16 \times 10^6$ cm/mol and of 10% (−*ac*, +*sc*) with $I(\text{calc}) = 0.39 \times 10^6$ cm/mol. This leads to a calculated summed intensity of $\{(0.6)0.16 + (0.1)0.39\} \times 10^6 = 0.135 \times 10^6$ cm/mol. This is to be compared to the calculated summed contributions of 15% (*sp*, −*sc*) with $I(\text{calc}) = 0.49 \times 10^6$ cm/mol and 15% (*sp*, +*sc*) with $I(\text{calc}) = 0.36 \times 10^6$ cm/mol, leading to $\{(0.15)0.49 + (0.15)0.36\} \times 10^6 = 0.128 \times 10^6$ cm/mol.

Using the ab initio frequencies, the more intense bands in the 1500−1200 cm^{-1} region can be straightforwardly assigned to modes of the dominant conformer. Near 1440 and 1380 cm^{-1} and between 1350 and 1280 cm^{-1}, weaker transitions are detected that we associate with higher energy conformers. For the same reasons as for the CH stretches, no detailed assignment of the bands of the higher energy conformers is attempted.

Figure 6b shows that between 1200 and 1120 cm^{-1} at least three transitions are present in the experimental spectrum: a hybrid with a (complex) Q branch at 1183 cm^{-1} and type-B contours with band centers at 1161 and 1144 cm^{-1}. Because in this region only one skeletal vibration in each conformer is predicted, the observation of three transitions supports the presence of several conformers in the sample. In agreement with the predictions, we assign the transition with the highest frequency, at 1183 cm^{-1}, to (+*ac*, −*sc*). This band is not the most intense of the observed triplet, which also here can be rationalized from the calculated intensities. For (*sp*, −*sc*) and (*sp*, +*sc*), the calculated intensities are much higher than that for (+*ac*, −*sc*), and therefore the bands at 1161 and 1144 cm^{-1} are assigned to these conformers. For the same mode in (−*ac*, +*sc*), the calculated intensity is merely half of that of (+*ac*, −*sc*), so that even when it is assumed that this conformer is present in the sample in a measurable fraction (10% by electron diffraction), its absence in this spectral region must be due to its weakness.

Between 1120 and 980 cm^{-1} six fundamentals are predicted for (+*ac*, −*sc*), whereas in the spectra, only four prominent bands are seen. The type-A transitions observed at 1105 cm^{-1} are assigned to the skeletal vibration predicted at 1096 cm^{-1}, and the type-B bands at 1046 and 995 cm^{-1} are assigned to the modes predicted at 1017 and 969 cm^{-1}, respectively. In this way, the mode predicted, with relatively weak intensity, at 1025 cm^{-1} remains unassigned. We associate it with the weak Q branch that can be detected at 1023 cm^{-1}. The most intense transition observed in this region, near 920 cm^{-1}, is assigned to the skeletal mode predicted at 909 cm^{-1}. This band has an unusual contour. At first sight, it reminds us of a type-B contour. However, the separation between the two maxima, 9 cm^{-1}, is too small to be the PQ−QR separation of a type-B band of the present compound and the low-frequency component at 923 $cm^{-1}$is too sharp to be the PQ branch. Therefore, the contour is interpreted as a type-A or type-C transition that is severely deformed by mechanical anharmonicity; i.e., it is a mode for which the rotational constants of the excited vibration state differ markedly from those of the ground state.[52] Thus, the maximum at 933 cm^{-1} is the R branch, and the 923 cm^{-1} component is the Q branch, with the P branch barely visible as a faint shoulder near 915 cm^{-1}. Such a pronounced anharmonic deformation is uncommon, but not impossible, for a fundamental skeletal vibration. It follows from the above interpretation that the band predicted, with relatively important intensity, at 942 cm^{-1}, remains to be assigned. To accept the absence in the experimental spectrum of bands attributable to this mode, it must be accepted that it is significantly weaker than predicted and remains unobserved under the 923 cm^{-1} band. Close inspection of the spectrum shows that especially near the higher three transitions in this region a number of weak Q branches can be observed. These are associated with the higher energy conformers. Also, here the complexity of the spectrum prevents a more detailed interpretation.

Table 4 shows that between 900 and 700 cm^{-1} for (+*ac*, −*sc*) a single fundamental is predicted, with low intensity at 813 cm^{-1} and that the corresponding mode in the other conformers should appear shifted to lower frequencies by 30−35 cm^{-1}. In this region of the observed spectrum, Figure 6c,

several weak transitions are detected. The more intense one at 834 cm^{-1} is assigned to (+*ac*, −*sc*), and the weaker ones at 825, 809, and 803 cm^{-1} are associated, in the calculated order, with the three higher energy conformers, i.e., with (−*ac*, +*sc*), (*sp*, −*sc*), and (*sp*, +*sc*), respectively. Note that this is a good indication for the presence of the rather elusive (−*ac*, +*sc*) form. Its appearance here is in line with its high $I(\text{calc}) = 1.30 \times 10^6$ cm/mol, much higher than the *I*(calc) values of the corresponding mode in the other conformers. It may also be remarked that, with the exception of the transition at 803 cm^{-1}, close to each of the above Q branches at least three weaker Q branches can be distinguished, which we assign as hot transitions.

The complex absorption observed between 620 and 510 cm^{-1} is shown in Figure 6d. In this region, a single fundamental skeletal vibration is calculated for each conformer. In view of the calculated frequencies, we assign the more intense type-B band in this region, with a band center at 532 cm^{-1}, to (+*ac*, −*sc*) and the weaker A/C hybrid, with a complex Q branch, at 595 cm^{-1} to (*sp*, −*sc*). Furthermore, two series of very weak C-type Q branches with decreasing intensities can be identified, the first with components at 579, 571, and 558 cm^{-1} and the other with components at 548, 539, and 526 cm^{-1}. These are assigned as torsional series superposed on the skeletal vibration involved, because of the (*sp*, +*sc*) and (−*ac*, +*sc*) conformers, respectively.

From the results discussed so far, we conclude that the vapor-phase IR spectrum shows BUO to occur as a mixture of several conformers. Because for many fundamentals the bands due to higher energy conformers are calculated as relatively weak, one conformer seems to dominate. The characteristics of the OH stretchings show that the dominant species has the (+*ac*, −*sc*) conformation. Our interpretation of the OH stretching region, and of the 870−770 and 620−510 cm^{-1} regions, indicates that in total four conformers have been detected. The data obtained do not allow a completely unambiguous identification of the three higher energy conformers, but they are most probably the first three higher energy conformers obtained from the DFT calculations: i.e., the (*sp*, −*sc*), (*sp*, +*sc*), and (−*ac*, +*sc*) conformers.

Table 4 summarizes the experimental and calculated IR data together with the assignments. The comparison shows that the root-mean-square deviation and the largest deviation between experimental and calculated wavenumbers for the (+*ac*, −*sc*) conformer are 13 and 29 cm^{-1}, respectively. A satisfactory, albeit more qualitative, agreement could be seen for the other rotamers. Figure 7 gives the comparison between the experimental gas-phase spectrum at room temperature and the calculated spectrum summed over the four lowest energy conformers with their abundancies given in Table 1. It follows that the agreement on frequencies is good and the agreement on relative intensities is also good, except that for ν(OH).

Electron Diffraction

The complexity of the gas-phase conformer mixture challenges the discriminating power of the electron-diffraction data and, hence, requires a careful choice of geometrical and vibrational model parameters and refinables.

To do so, we computed for the (+*ac*, −*sc*), (*sp*, −*sc*), (*sp*, +*sc*), and (−*ac*, +*sc*) conformers the vibrational amplitudes u_{ij} and the perpendicular vibrational amplitudes K_{ij} of the interatomic distances. For this, we used a program devised by Sipachev[53] and the IR-scaled B3LYP/6-31G** force field. The program provides the corrections for the Bastiansen−Morino shrinkage effect while extending the theory described by

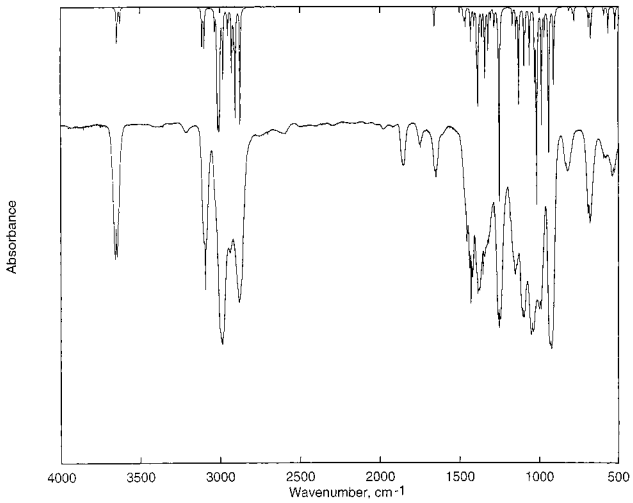

Figure 7. Comparison between the experimental (bottom) gas-phase IR spectrum of BUO recorded at room temperature and the calculated (top) IR spectrum composed of the Boltzmann weighted spectra with Gaussian band types of the four lowest energy conformers.

Cyvin.[54] Unlike the standard procedure to convert an r_α structure to an r_a structure, the algorithm by Sipachev takes into account also other second-order terms with respect to the displacements from the equilibrium positions that appear when solving the vibrational problem in the harmonic approximation. In agreement with physical intuition, and unlike the conventional procedure,[54] the calculations by the new scheme[53] give zero or negligibly small corrections for bonded and short nonbonded distances and large corrections for long interatomic distances depending on a number of vibrational coordinates and, therefore, are more liable to distortions resulting from vibrational effects. The vibrational amplitudes u_{ij} and their perpendicular counterparts K_{ij}, so obtained, are given in Table 5.

Geometrical models of the four conformers were constructed as defined in Table 6. The refinable parameters (r, θ) and the constraints were chosen after a scrutiny of Table 2 and after conversion to the r_α basis ($r_\alpha = r_g - K$), remembering that B3LYP/6-31G** distances were found to be close to those of r_g geometry. Then, a provisional refinement by an iterated step-by-step procedure[55] was performed separately for each of the four conformers. As refinables, nine geometrical parameters ((r, θ); Table 6) and six vibrational amplitudes (u) were taken and assigned to the six groups of interatomic distances denoted in Table 5 by A−F. Within each group, the vibrational parameters were constrained to the corresponding refinable using constraint values taken from Table 5. The u_{ij} values of the other distances were fixed to their calculated values. To start with, the step-by-step approach was chosen because strong correlations between certain r, θ, and u refinables exist and because the use of calculated absolute values, considerd less accurate than calculated differences between similar parameters, may lead to initial models far from the final ones and to high disagreement values, R. Under such conditions, conventional least-squares procedures often perform poorly. After about 20 iterations per conformer, the step-by-step refinements were considered complete, and as a first test of the discriminating power, we compared the radial distribution functions, rdf, of the four lowest energy conformers obtained at this point in the analysis. The rdf curves of these *provisional models* are to be compared with the radial distribution curve directly obtained from the experimental diffraction intensities rdf(exp). From these curves and the four difference curves, rdf(exp)−rdf(provisional model), presented in Figure 8, it may seem that no discrimination can

TABLE 5: Amplitudes of Vibration and Perpendicular Corrections Calculated in Angstroms for the BUO Conformers[a]

	(+*ac*, −*sc*)		(*sp*, −*sc*)		(*sp*, +*sc*)		(−*ac*, +*sc*)	
	u_{ij}	K_{ij}	u_{ij}	K_{ij}	u_{ij}	K_{ij}	u_{ij}	K_{ij}
C2−C1	0.050	0.0017	0.051	0.0017	0.051	0.0017	0.051	0.0017
C3−C2	0.050	0.0016	0.050	0.0016	0.050	0.0017	0.050	0.0016
C4−C3	0.040	0.0012	0.040	0.0012	0.040	0.0012	0.040	0.0012
O5−C2	0.048	0.0016	0.048	0.0016	0.048	0.0016	0.048	0.0016
O5−H7	0.068	0.0048	0.068	0.0048	0.068	0.0048	0.068	0.0048
C1−H11	0.076	0.0053	0.076	0.0053	0.076	0.0053	0.076	0.0053
C1−H12	0.076	0.0053	0.076	0.0053	0.076	0.0053	0.076	0.0053
C1−H13	0.076	0.0053	0.076	0.0053	0.076	0.0053	0.076	0.0053
C2−H6	0.078	0.0055	0.078	0.0055	0.077	0.0054	0.077	0.0054
C3−H8	0.075	0.0052	0.075	0.0052	0.075	0.0052	0.075	0.0052
C4−H9	0.075	0.0052	0.075	0.0052	0.075	0.0052	0.075	0.0052
C4−H10	0.075	0.0052	0.075	0.0052	0.075	0.0052	0.075	0.0052
C1···O5	A 0.068	0.0053	A 0.068	0.0053	0.068	0.0051	A 0.068	0.0052
C1···H6	0.106	0.0097	0.106	0.0097	0.106	0.0097	0.105	0.0096
C1···C3	A 0.074	0.0058	A 0.074	0.0058	0.073	0.0057	A 0.068	0.0052
C1···H7	D 0.095	0.0291	D 0.094	0.0297	0.182	0.0096	D 0.179	0.0119
C1···H8	C 0.164	0.0130	B 0.167	0.0165	0.157	0.0084	C 0.101	0.0268
C1···C4	B 0.123	0.0213	C 0.126	0.0190	0.105	0.0198	B 0.102	−0.0040
C1···H9	E 0.209	0.0378	B 0.220	0.0352	0.177	0.0356	E 0.182	−0.0162
C1···H10	B 0.152	0.0348	D 0.150	0.0323	0.140	0.0322	E 0.124	0.0148
C2···H11	F 0.107	0.0115	F 0.107	0.0115	0.108	0.0116	F 0.107	0.0116
C2···H12	F 0.107	0.0114	F 0.107	0.0116	0.107	0.0115	F 0.108	0.0117
C2···H13	F 0.107	0.0115	F 0.107	0.0115	0.108	0.0116	F 0.107	0.0115
C2···H7	F 0.100	0.0079	F 0.100	0.0080	0.100	0.0080	F 0.100	0.0079
C2···H8	F 0.103	0.0118	F 0.104	0.0116	0.103	0.0115	F 0.103	0.0116
C2···C4	D 0.065	0.0072	D 0.062	0.0069	0.062	0.0069	D 0.062	0.0068
C2···H9	B 0.145	0.0167	B 0.143	0.0168	0.143	0.0167	B 0.140	0.0156
C2···H10	C 0.096	0.0211	C 0.096	0.0207	0.095	0.0206	C 0.096	0.0207
C3···O5	A 0.069	0.0054	A 0.063	0.0048	0.063	0.0047	A 0.068	0.0052
C3···H7	D 0.176	0.0057	D 0.174	0.0063	0.182	0.0097	D 0.181	0.0086
C3···H6	F 0.104	0.0096	F 0.105	0.0097	0.106	0.0098	F 0.106	0.0097
C3···H11	0.169	0.0141	0.166	0.0126	0.163	0.0126	0.102	0.0226
C3···H12	0.163	0.0125	0.163	0.0138	0.165	0.0145	0.157	0.0130
C3···H13	A 0.102	0.0249	A 0.102	0.0241	0.102	0.0238	A 0.156	0.0131
C3···H9	F 0.096	0.0126	F 0.097	0.0127	0.097	0.0127	F 0.096	0.0125
C3···H10	F 0.096	0.0123	F 0.096	0.0125	0.096	0.0124	F 0.096	0.0124
C4···H8	F 0.096	0.0112	F 0.096	0.0110	0.096	0.0111	F 0.096	0.0112
C4···H6	0.144	0.0025	0.122	0.0215	0.140	0.0212	0.138	0.0235
C4···O5	C 0.123	0.0216	B 0.101	0.0023	0.099	0.0008	B 0.116	0.0232
C4···H7	D 0.247	0.0113	0.241	0.0068	0.251	0.0097	B 0.252	0.0179
C4···H11	0.245	0.0227	B 0.203	0.0352	0.179	0.0347	E 0.120	0.0217
C4···H12	0.195	0.0393	B 0.239	0.0204	0.222	0.0248	0.218	−0.0022
C4···H13	B 0.136	0.0396	F 0.143	0.0384	0.127	0.0374	D 0.222	0.0005
O5···H6	F 0.100	0.0089	F 0.100	0.0089	0.101	0.0090	F 0.102	0.0090
O5···H8	B 0.170	0.0149	C 0.098	0.0231	0.097	0.0242	C 0.167	0.0102
O5···H9	B 0.212	0.0387	E 0.185	−0.0016	0.182	−0.0055	E 0.199	0.0411
O5···H10	A 0.149	0.0353	B 0.123	0.0200	0.122	0.0189	B 0.145	0.0357
O5···H11	A 0.098	0.0247	A 0.098	0.0243	0.099	0.0233	A 0.162	0.0125
O5···H12	0.175	0.0167	0.173	0.0164	0.165	0.0159	0.099	0.0229
O5···H13	0.171	0.0137	0.169	0.0142	0.164	0.0130	0.163	0.0160
H6···H7	0.180	0.0127	0.180	0.0117	0.118	0.0330	0.119	0.0313
H7···H8	0.276	0.0347	0.191	0.0217	0.200	0.0264	0.282	0.0350
H7···H9	0.332	0.0295	0.305	0.0145	0.307	0.0123	0.330	0.0364
H7···H10	0.277	0.0223	0.260	0.0165	0.273	0.0203	0.283	0.0283
H7···H11	0.130	0.0427	0.130	0.0429	0.180	0.0281	0.270	0.0403
H7···H12	0.187	0.0441	0.184	0.0456	0.261	−0.0041	0.178	0.0298
H7···H13	0.179	0.0432	0.181	0.0435	0.278	0.0398	0.258	0.0005
H6···H8	0.122	0.0296	0.172	0.0136	0.180	0.0206	0.178	0.0164
H6···H9	0.215	−0.0044	0.181	0.0362	0.221	0.0366	0.209	0.0394
H6···H10	0.159	0.0195	0.151	0.0335	0.160	0.0335	0.161	0.0352
H6···H11	0.180	0.0166	0.181	0.0174	0.179	0.0171	0.173	0.0163
H6···H12	0.124	0.0284	0.124	0.0280	0.124	0.0276	0.178	0.0169
H6···H13	0.175	0.0163	0.174	0.0155	0.175	0.0160	0.124	0.0271
H8···H9	0.117	0.0254	0.117	0.0254	0.117	0.0255	0.117	0.0253
H8···H10	0.163	0.0191	0.163	0.0189	0.163	0.0189	0.163	0.0188
H8···H11	0.265	0.0378	0.253	0.0064	0.233	−0.0069	0.138	0.0415
H8···H12	0.245	−0.0016	0.247	0.0379	0.267	0.0321	0.173	0.0378
H8···H13	0.176	0.0352	0.177	0.0353	0.165	0.0304	0.183	0.0385
H9···H10	0.118	0.0162	0.118	0.0163	0.118	0.0163	0.118	0.0161
H9···H11	0.341	0.0424	0.251	0.0591	0.199	0.0578	0.198	0.0128
H9···H12	0.230	0.0643	0.339	0.0378	0.295	0.0440	0.304	−0.0160
H9···H13	0.230	0.0500	0.245	0.0500	0.207	0.0476	0.327	−0.0022
H10···H11	0.274	0.0338	0.242	0.0438	0.225	0.0428	0.138	0.0418
H10···H12	0.241	0.0494	0.263	0.0322	0.254	0.0347	0.234	0.0131
H10···H13	0.154	0.0585	0.157	0.0561	0.148	0.0547	0.237	0.0153
H11···H12	0.123	0.0151	0.123	0.0151	0.123	0.0151	0.123	0.0150
H11···H13	0.123	0.0151	0.123	0.0151	0.123	0.0150	0.123	0.0149
H12···H13	0.122	0.0150	0.122	0.0150	0.122	0.0149	0.123	0.0150

[a] Terms with equal letters (A−F) were refined in groups.

TABLE 6: Model Construction with Refinable Geometric Parameters and Constraints

parameter[a]	for all conformers	parameter[a]	for all conformers
⟨C−H⟩[b]	1.088	C3−C2−C1	$\theta 2$
C2−C1	$r1$	C3−C2−O5	$\theta 3$
C3−C2	$r1-0.02$	H9−C4−H10	116.9
C4−C3	$r2$	C4−C3−H8	120.0
O5−C2	$r3$	C2−O5−H7	107.0
C2−H6	1.100	C2−C1−H11	110.0
O5−H7	$r4$	C3−C2−H6	108.3
⟨C−H⟩[c]	$r5$	C1−C2−O5	$\theta 4$
C4−C3−C2	$\theta 1$	C1−C2−H6	110.5

[a] For the numbering scheme, see Figure 1. [b] C4−H9 and C4−H10. [c] C1−H11, C1−H12, and C1−H13.

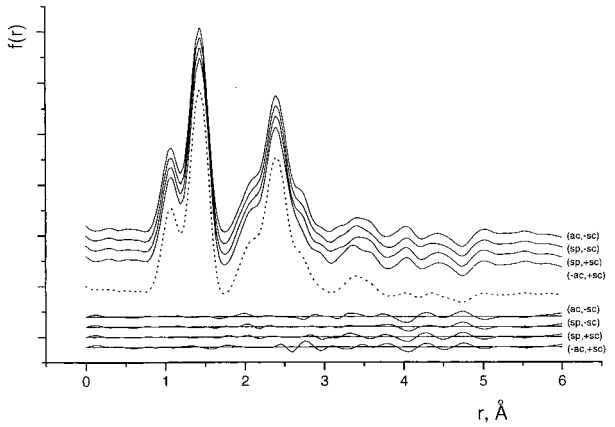

Figure 8. Radial distribution curves, rdf(provisional model), of the four lowest energy conformers (top four curves) compared with the experimental radial distribution curve, rdf(exp), of BUO (middle, - - -). The four corresponding difference curves, rdf(exp)−rdf(provisional model), are also given (bottom four curves). See the text for explanation.

be expected between the (*sp*, −*sc*) and (*sp*, +*sc*) forms, but a discrimination between three forms seems possible. Therefore, we set out to rigorously test the discriminating power of the diffraction intensities for a mixture of the (+*ac*, −*sc*), (−*ac*, +*sc*), and (*sp*, −*sc*) conformers. In this test, the (*sp*, −*sc*) form is given double weight to incorporate the (electron-diffraction-invisible) (*sp*, +*sc*) form of quasiequal energy. Using the final step-by-step models, we calculated a set of disagreement factors for various conformer ratios. We changed the percentages of the three conformers in the mixture from 0 to 100% in steps of 5%, taking all 232 possibilities into account. To discriminate between these mixtures, we compared the ratio of the *R* values of two such mixtures with tabulated[56] values of Q (p, $n - p$, α), in which p denotes the degree of freedom (here 3, i.e., the number of conformers in the mixture), n the number of data points (here 130), and α the chosen level of significance. If the *R* value ratio is larger that of Q, then one rejects the hypothesis at the 100α% significance level that the test mixtures under consideration are equal.

Performing these tests at the 5% level of significance, we concluded that the electron-diffraction data can be described by BUO existing in the gas phase of three conformers with the following intervals: (+*ac*, −*sc*), 60 ± 20%; (*sp*, −*sc*) and (*sp*, +*sc*), 20 ± 20%; (−*ac*, +*sc*), 20 ± 20%.

At this point, we considered the model sufficiently close to the final one, and a least-squares analysis was performed, taking the nine geometrical parameters (Table 6), six (groups of) vibrational amplitudes (Table 5), and three conformer percentages as refinables, while keeping the other parameters fixed at their calculated values. Table 7 summarizes the results. We conclude that bond lengths and valence angles averaged over the conformers are within error limits with the B3LYP values. Moreover, the best set of conformer percentage was found to be (+*ac*, −*sc*), 58 ± 23%; (*sp*, −*sc*) and (*sp*, +*sc*), 32 ± 23%; and (−*ac*, +*sc*), 10 ± 23%.

TABLE 7: Results of Electron-Diffraction Least-Squares Refinement with the Estimated Standard Deviation (5 Times σ from Least Squares) in Parentheses

Geometrical Parameters

	r_g bond lengths (Å), valence angles (deg)
C2−C1 ($r1$)	1.504(9)
C3−C2 ($r1-0.02$)	1.484(9)
C4−C3 ($r2$)	1.327(9)
O5−C2 ($r3$)	1.421(9)
O5−H7 ($r4$)	0.982(21)
⟨C−H⟩ ($r5$)	1.117(15)
C4−C3−C2 ($\theta 1$)	126(1)
C3−C2−C1 ($\theta 2$)	110(1)
C3−C2−O5 ($\theta 3$)	109(1)
C1−C2−O5 ($\theta 4$)	110(1)

Vibrational Parameters

	(+*ac*, −*sc*) u_{ij}	(*sp*, −*sc*) u_{ij}	(−*ac*, +*ac*) u_{ij}
C1···O5	0.082(25)	0.082(25)	0.082(25)
C1···C3	0.088(25)	0.088(25)	0.082(25)
C1···C4	0.163(60)	0.103(45)	0.142(60)
C2···C4	0.059(26)	0.057(26)	0.057(26)
C3···O5	0.083(25)	0.077(25)	0.082(25)
C4···O5	0.099(45)	0.141(60)	0.157(60)

abundance	percentages
(+*ac*, −*sc*)	58
(*sp*, −*sc*) and (*sp*, +*sc*) together	32
(−*ac*, +*sc*)	10
final *R* value (%)	6.55

It may be argued that these abundance percentages do not exactly correspond to room temperature, the temperature of the sample. In fact, introduction of a sample into an electron-diffraction chamber results at least in a mild supersonic expansion. Although vibrational cooling is often insignificant for polyatomic molecules, the low-energy separation between the various conformers may lead to a distribution in the electron-diffraction chamber that is slightly cooler than that for the spectroscopic measurements. We believe, however, that this effect is covered by the 5σ error limits given. Moreover, the percentages taken in the analysis of the spectroscopic data were essentially used in a semiquantitative manner. Finally, despite the large error limits, these observed percentages are in fair agreement with the B3LYP values.

Conclusions

The existence in the gas phase of four BUO conformers followed from analyses of electron-diffraction data and of IR frequencies and intensity band profiles both measured at 20 °C. This number of low-energy conformers makes the conformational analysis of BUO one of the most complex ever successfully completed. Results of force field and geometry calculations at the B3LYP/6-31G** level played an essential role in the interpretation of the experimental data. Given in order of increasing energy, the conformers are (+*ac*, −*sc*) < (*sp*, −*sc*) ≤ (*sp*, +*sc*) < (−*ac*, +*sc*). It follows that in a greater or less degree the bonds C2−H, C2−OH, and C2−CH_3 may eclipse

the C═C bond. In this aspect, BUO can be considered as an intermediate between allyl alcohol[7−9] and 1-butene.[10,11] In all four BUO conformers, the OH bond points toward the C═C bond, indicating the presence of an attractive, intramolecular OH/C═C interaction, as was previously suggested,[1−3] but could not be experimentally substantiated at that time. In this, BUO parallels the behavior seen in allyl alcohol.

In fact, the conformational characteristics as well as the geometrical details of the conformers can be visualized by attractive (hyper)conjugative effects modified by repulsive steric interactions. Attractive (eclipse rule) and repulsive (generalized trans rule[47]) interactions have numerous consequences on bond lengths and valence angles, as well as on OH and other vibration frequencies. They are revealed by the B3LYP calculations and follow the expected trends. A fair agreement exists between the B3LYP-calculated relative conformer percentages (Table 1) and those of the experimental ones (Table 7) from the final electron-diffraction model. It proved very advantageous to scale the four B3LYP/6-31G**-calculated force fields using just the three transferable[49] scale factors for stretching, bending, and torsion constants. These scaled force fields allowed us to identify the IR bands indicating the conformational equilibrium and led to an almost straightforward assignment of the fundamental IR frequencies.

Acknowledgment. The authors express their gratitude to Professor Ludmila V. Khristenko (Moscow) for the calculation of u_{ij} values and to Professor Lev Vilkov (Moscow) for some valuable remarks. C.V.A. and W.A.H. thank the Flemish Science Foundation (FWO Vlaanderen) for an appointment as "onderzoeksdirecteur" and as "post-doctoraal medewerker", respectively. I.F.S. is thankful to the Special Research Fund of Antwerpen University for a postdoctoral fellowship and to the Russian RFBR (Project No. 99-32511a) for financial support. O.N.K. is grateful for postdoctoral grants given by "De Diensten van de eerste Minister, DWTC" in 1997 and 1998. Financial support to the UIA laboratory by the University of Antwerpen under Grant GOA-BOF-UA No. 23 and by the Flemish Organization IWT under Grant ITA II is gratefully acknowledged.

References and Notes

(1) Smith, Z.; Carballo, N.; Wilson, E. B.; Marstokk, K.-M.; Møllendal, H. *J. Am. Chem. Soc.* **1985**, *107*, 1951.
(2) Kahn, S. D.; Pau, C. F.; Chamerlin, A. R.; Hehre, W. J. *J. Am. Chem. Soc.* **1987**, *109*, 650.
(3) Kahn, S. D.; Hehre, W. J. *J. Am. Chem. Soc.* **1987**, *109*, 666.
(4) Arnaud, P.; Armand, Y. *C. R. Hebd. Seances Acad. Sci.* **1961**, *253*, 1547.
(5) Armand, Y.; Arnaud, P. *Ann. Chim. (Paris)* **1964**, *9*, 433.
(6) IUPAC. *Nomenclature of Organic Chemistry*, Section E: Stereochemistry, Recommendations; Pergamon Press: Oxford, U.K., 1974.
(7) Murty, A. N.; Curl, R. F., Jr. *J. Chem. Phys.* **1967**, *46*, 4176.
(8) Horn, A.; Marstokk, K.-M.; Møllendal, H.; Priebe, H. *Acta Chem. Scand.* **1983**, *A37*, 679.
(9) Vanhoutegem, F.; Pyckhout, W.; Van Alsenoy, C.; Van den Enden, L.; Geise, H. J. *J. Mol. Struct.* **1986**, *140*, 33.
(10) Kondo, S.; Hirota, E.; Morino, Y. *J. Mol. Spectrosc.* **1968**, *28*, 471.
(11) Van Hemelrijk, D.; Van den Enden, L.; Geise, H. J.; Sellers, H. L.; Schäfer, L. *J. Am. Chem. Soc.* **1980**, *102*, 2189.
(12) Geise, H. J.; Pyckhout, W. In *Stereochemical Application of Gas-Phase Electron Diffraction*; Hargittai, I., Hargittai, M., Eds.; VCH Publishers: Deerfield Beach, FL, 1988; Vol. 1, Chapter 10.
(13) Schäfer, L.; Ewbank, J. D.; Siam, K.; Chiu, N. S.; Sellers, H. L. In *Stereochemical Application of Gas-Phase Electron Diffraction*; Hargittai, I., Hargittai, M., Eds.; VCH Publishers: Deerfield Beach, FL, 1988; Vol. 1, Chapter 9.
(14) Schäfer, L. *J. Mol. Struct.* **1983**, *100*, 51.
(15) Pyckhout, W.; Horemans, N.; Van Alsenoy, C.; Geise, H. J.; Rankin, D. W. H. *J. Mol. Struct.* **1987**, *156*, 315.
(16) Pyckhout, W.; Van Alsenoy, C.; Geise, H. J.; Van der Veken, B.; Pieters, G. *J. Mol. Struct.* **1985**, *130*, 335.
(17) Pyckhout, W.; Van Alsenoy, C.; Geise, H. J.; Van der Veken, B.; Coppens, P.; Traetteberg, M. *J. Mol. Struct.* **1986**, *147*, 85.
(18) De Smedt, J.; Vanhouteghem, F.; Van Alsenoy, C.; Geise, H. J.; Van der Veken, B.; Coppens, P. *J. Mol. Struct.* **1989**, *195*, 227.
(19) Wang, Y.; De Smedt, J.; Coucke, J.; Van Alsenoy, C.; Geise, H. J. *J. Mol. Struct.* **1993**, *299*, 43.
(20) Mack, H. G.; Oberhammer, H. *THEOCHEM* **1992**, *258*, 197.
(21) De Smedt, J.; Vanhouteghem, F.; Van Alsenoy, C.; Geise, H. J.; Schäfer, L. *THEOCHEM* **1992**, *259*, 289.
(22) Peng, Z. H.; Shlykov, S.; Van Alsenoy, C.; Geise, H. J.; Sluyts, E.; Van der Veken, B. *J. Phys. Chem.* **1995**, *99*, 10201.
(23) Wu, G.; Shlykov, S.; Van Alsenoy, C.; Geise, H. J.; Sluyts, E.; Van der Veken, B. J. *J. Phys. Chem.* **1995**, *99*, 8589.
(24) Wu, G.; Shlykov, S.; Van Alsenoy, C.; Geise, H. J.; Sluyts, E.; Van der Veken, B. J. *J. Phys. Chem.* **1996**, *100*, 11620.
(25) Shlykov, S.; Tremmel, J.; Van Loock, J.; Geise, H. J. *J. Mol. Struct.* **1997**, *413*−*414*, 579.
(26) Tamagawa, K.; Iijima, T.; Kimura, M. *J. Mol. Struct.* **1976**, *30*, 243.
(27) Van Loock, J.; Van den Enden, L.; Geise, H. J. *J. Phys. E: Sci. Instrum.* **1983**, *16*, 255.
(28) Forster, H. R. *J. Appl. Phys.* **1970**, *41*, 5344.
(29) Ross, A. W.; Fink, M.; Hilderbrandt, R. *International Tables for Crystallography;* Kluwer Academic Publishers: Dordrecht, The Netherlands, 1992; Vol. 4, p 245.
(30) Tavard, C.; Nicolas, D.; Rouault, M. *J. Chim. Phys.-Chim. Biol.* **1964**, *40*, 1686.
(31) Van den Enden, L.; Van Laere, E.; Geise, H. J.; Mylhoff, F. C.; Spelbos, A. *Bull. Soc. Chim. Belg.* **1976**, *85*, 735.
(32) Pulay, P. *Mol. Phys.* **1969**, *17*, 197.
(33) Pulay, P. *Theor. Chim. Acta* **1979**, *50*, 299.
(34) Pulay, P. In *Modern Theoretical Chemistry*; Schäfer, H. F., III, Ed.; Plenum Press: New York, 1977; Vol. 4, p 154 ff.
(35) Van Alsenoy, C.; Peeters, A. *THEOCHEM* **1993**, *286*, 18.
(36) Frisch, M. J.; Trucks, G. W.; Schlegel, H. B.; Gill, P. M. W.; Johnson, B. G.; Robb, M. A.; Cheeseman, J. R.; Keith, T.; Petersson, G. A.; Montgomery, J. A.; Raghavachari, K.; Al-Laham, M. A.; Zakrzewski, V. G.; Ortiz, J. V.; Foresman, J. B.; Cioslowski, J.; Stefanov, B. B.; Nanayakkara, A.; Challacombe, M.; Peng, C. Y.; Ayala, P. Y.; Chen, W.; Wong, M. W.; Andres, J. L.; Replogle, E. S.; Gomperts, R.; Martin, R. L.; Fox, D. J.; Binkley, J. S.; Defrees, D. J.; Baker, J.; Stewart, J. P.; Head-Gordon, M.; Gonzalez, C.; Pople, J. A. *Gaussian 94*, revision D.4; Gaussian, Inc.: Pittsburgh, PA, 1995.
(37) Aspiala, A.; Lotta, T.; Murto, J.; Räsänen, M. *J. Chem. Phys.* **1983**, *79*, 4183.
(38) Pulay, P.; Fogarasi, G.; Pang, F.; Boggs, J. E. *J. Am. Chem. Soc.* **1979**, *101*, 2550.
(39) Ditchfield, R.; Hehre, W. J.; Pople, J. A. *J. Chem. Phys.* **1971**, *54*, 724.
(40) Hehre, W. J.; Ditchfield, R.; Pople, J. A. *J. Chem. Phys.* **1972**, *56*, 2257.
(41) Becke, A. D. *Phys. Rev. A: At., Mol., Opt. Phys.* **1988**, *38*, 3098.
(42) Lee, C.; Yang, W.; Parr, R. G. *Phys. Rev. B: Condens. Matter* **1988**, *37*, 785.
(43) Becke, A. D. *J. Chem. Phys.* **1993**, *98*, 5648.
(44) Becke, A. D. *J. Chem. Phys.* **1996**, *104*, 1040.
(45) Becke, A. D. In *Modern Electronic Structure Theory*; Yarkony, D. R., Ed.; World Scientific: Singapore, Singapore, 1995.
(46) Schäfer, L. *J. Mol. Struct.* **1983**, *100*, 51.
(47) Murto, J.; Räsänen, M.; Aspiala, A.; Homanen, L. *J. Mol. Struct.* **1983**, *92*, 45.
(48) Nishio, M.; Hirota, M.; Umezawa, Y. *The CH/*Π *interaction*; Wiley-VCH: New York, 1998.
(49) Rauhut, G.; Pulay, P. *J. Phys. Chem.* **1995**, *99*, 3093.
(50) Van der Veken, B. J. In *Computing Applications in Molecular Spectroscopy*; George, W. O., Steele, D., Eds.; The Royal Society of Chemistry: Cambridge, U.K., 1995; pp 105−179.
(51) Van der Veken, B. J.; Herrebout, W. A.; Liefooghe, H. H. *J. Mol. Struct.* **1992**, *268*, 293.
(52) Van der Veken, B. J. In *Vibrational Spectra and Structure, A Series of Advances, Vol. 15*; Durig, J. R., Ed.; Elsevier: Amsterdam, The Netherlands, 1986; pp 313−400.
(53) Sipachev, V. A. *Advances in Molecular Structure Research*; JAI Press: New York, 1999; Vol. 5, pp 263−311.
(54) Cyvin, S. J. *Molecular Vibrational and Mean Square Amplitudes*; Universitet Forlaget: Oslo, Norway, 1968.
(55) Sadova, N. I.; Ivanov, A. A.; Popik, M. V.; Shishkov, I. F.; Vilkov, L. V.; Pankrushev, Yu. A. *Zh. Strukt. Khim.* **1989**, *30*, 56.
(56) Hamilton, W. C. *Statistics in Physical Science; Estimation, Hypothesis Testing and Least-Squares*; Roland Press Co.: New York, 1964.